Spin-Dependent Cooper Pair Phase and Pure Spin Supercurrents in Strongly Polarized Ferromagnets

R. Grein, M. Eschrig, G. Metalidis, and Gerd Schön

Institut für Theoretische Festkörperphysik and DFG-Center for Functional Nanostructures, Universität Karlsruhe, D-76128 Karlsruhe, Germany

(Received 20 March 2009; published 4 June 2009)

We study heterostructures of singlet superconductors and strongly spin-polarized ferromagnets and show that a relative phase arises between the superconducting proximity amplitudes in the two ferromagnetic spin bands. We find a tunable pure spin supercurrent in a spin-polarized ferromagnet contacted with only one superconductor electrode. We show that Josephson junctions are most effective for a spin polarization $P \sim 0.3$, and that critical currents for positive and negative bias differ for a high transmission Josephson junction, due to a relative phase between single and double pair transmission.

DOI: 10.1103/PhysRevLett.102.227005 PACS numbers: 74.50.+r, 72.25.Mk, 74.78.Fk, 85.25.Cp

Superconductor (SC)/ferromagnet (FM) hybrid structures have triggered considerable research activities in recent years [1–11]. In particular, FM Josephson junctions are promising spintronics devices as they allow for tuning the critical current via the electron spin. However, due to the competition between the uniform spin alignment in the FM and spin-singlet pairing in the SC, singlet superconducting correlations decay in the FM on a much shorter length scale than in a normal metal [12]. Although this results in a rapidly decaying Josephson current for long junctions, the proximity effect leads to interesting physics in short and/or weakly polarized junctions, e.g., oscillations of the supercurrent as a function of the thickness of the interlayer that can give rise to π-junction behavior [12,13]. Recently, however, in contradiction with these expectations, long-range supercurrents have been reported through strongly spin-polarized materials [6]. Theoretical calculations have shown that for strongly polarized ferromagnets (SFMs) spin scattering at SC/FM interfaces [14] leads to a transformation of singlet correlations in the SC into triplet correlations [3] (the ''triplet reservoirs'' of Ref. [9]), which can carry a long-range supercurrent through the SFM [3,7–11].

So far, transport calculations in SC/FM hybrids have mostly concentrated on either fully polarized FMs, so-called half metals, or on the opposite limit of weakly polarized systems. However, most FMs have an intermediate exchange splitting of the energy bands of the order of 0.2–0.8 times the Fermi energy E_F. For this intermediate range, one could naively expect a behavior similar to two shunted half metallic junctions. We will show, using a microscopic interface model, that this picture is inadequate, and point out the crucial role played by the interfaces in coupling the SFM spin bands.

In this Letter, we study Josephson junctions with a strongly polarized interlayer, and find fundamental differences compared to both half metallic and weakly polarized interlayers. In particular, we see that, although correlations between ↑ and ↓ electrons are suppressed due to the strong exchange field, spin-active interfaces generate interactions between long-range triplet supercurrents in the two spin bands. We find that the long-range critical Josephson current varies nonmonotonically with spin polarization P, showing a maximum around $P = 0.3$. Furthermore, specifically when the exchange splitting is strong, additional phases arising from the interfaces [14] lead to different current-phase relations for the spin-resolved currents $I_\uparrow$ and $I_\downarrow$ through the junction. We show how this gives rise to (i) a relative phase between single pair and ''crossed'' two-pair transmission [the latter process is illustrated in Fig. 1(a), with equal numbers of pairs transferred in the spin ↑ and spin ↓ band], (ii) different critical Josephson currents for opposite bias, (iii) equilibrium shifts in the current-phase relation, in contrast to previous predictions [9], and (iv) a tunable spin supercurrent in a FM brought into contact with a single SC electrode (we propose an experiment to measure this remarkable effect).

Quasiclassical Green's functions (QCGFs) [15,16] are a powerful tool to describe hybrid structures of superconductors and nonsuperconducting materials. Consider, e.g., the interface between a SC and a SFM shown in Fig. 1(b). For trajectories on the SC side, labeled 1, and character-

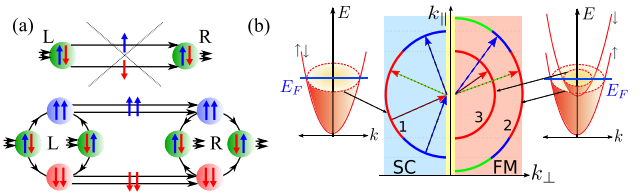

FIG. 1 (color online). (a) The coherent transfer of singlet pairs via a SFM (top) is not possible. However, the ''crossed'' pair transmissions process (bottom) is possible and leads to intriguing effects in high transmission junctions. (b) SC/SFM interface, showing the Fermi surfaces on either side (thick lines). Assuming momentum conservation parallel to the interface ($\vec{k}_\parallel$), a quasiparticle incident from the SC can either scatter into two (dotted arrows) or into only one (dashed arrows) spin band of the FM.

ized by Fermi momentum $\vec{p}_{F1}$ and Fermi velocity $\vec{v}_{F1}$, the QCGF is obtained from the microscopic one, $\hat{G}$, by integrating out the components oscillating on the Fermi wavelength scale $\lambda\!\!\!^{-}_{F1} = \hbar/p_{F1}$: $\hat{g}(\vec{p}_{F1}, \vec{R}, \varepsilon, t) = \int d\xi_p \hat{\tau}_3 \hat{G}(\vec{p}, \vec{R}, \varepsilon, t)$, where $\xi_p = \vec{v}_{F1}(\vec{p} - \vec{p}_{F1})$. The QCGF, $\hat{g}$, then varies as a function of the spatial coordinate $\vec{R}$ at a scale set by the superconducting coherence length $\xi_0 = \hbar v_{F1}/2\pi k_B T_c$, and obeys the Eilenberger equation

$$i\hbar\vec{v}_{F1} \cdot \nabla_{\vec{R}} \hat{g} + [\varepsilon\hat{\tau}_3 - \hat{\Delta} - \hat{h}, \hat{g}] = \hat{0}, \qquad (1)$$

with normalization condition $\hat{g}^2 = -\pi^2\hat{1}$ [16]. Here, the hat denotes the 2×2 Nambu matrix structure in particle-hole space, and $\hat{\tau}_3$ is the third Pauli matrix; $\hat{h}$ includes all mean field and self-energy terms governing the quasiparticle motion along QC trajectories aligned with $\vec{v}_{F1}$, and labeled by $\vec{p}_{F1}$; $\hat{\Delta}$ is the SC order parameter.

The exchange field $J_{\rm FM}$ in a SFM is comparable to the Fermi energy. As opposed to the weak polarization limit ($J_{\rm FM} \ll E_F$), this cannot be described by a term $-\vec{J}_{\rm FM} \cdot \vec{\sigma}$ (with $\vec{\sigma}$ the vector of Pauli spin matrices) in $\hat{h}$ of Eq. (1), because the QC approximation in this case neglects terms of order $J_{\rm FM}^2/E_F$ compared to Δ. In most SCs, this is not justified for $J_{\rm FM} > 0.1E_F$. However, for sufficiently large $J_{\rm FM} \gg \sqrt{E_F\Delta}$ the coherent coupling of the spin bands in the FM can be disregarded. Consequently, we define an independent QCGF for each spin band $\eta \in \{2, 3\}$ in Fig. 1(b): $\hat{g}(\vec{p}_{F\eta}, \vec{R}, \varepsilon, t) = \int d\xi_{p\eta} \hat{\tau}_3 \hat{G}(\vec{p}, \vec{R}, \varepsilon, t)$, where $\xi_{p\eta} = \vec{v}_{F\eta}(\vec{p} - \vec{p}_{F\eta})$. The exchange field is incorporated by the different Fermi velocities $\vec{v}_{F\eta}$ and momenta $\vec{p}_{F\eta}$ in the two spin bands, and does not enter the equation of motion (1) for the QCGFs. The $\hat{g}$ are Nambu matrices with diagonal (g) and off-diagonal (f) components. These components are spin scalar, as opposed to the QCGF in the SC where they form a 2×2 spin matrix as a result of spin coherence. Indeed, the spins of the pair wave function in the FM are fixed either to $|\uparrow\uparrow\rangle$ [band 2 in Fig. 1(b)] or to $|\downarrow\downarrow\rangle$ (band 3).

The interface enters the QC theory in the form of effective boundary conditions [17–19] connecting the incident and outgoing QCGFs for the three Fermi-surface sheets $\eta \in \{1, 2, 3\}$. The boundary conditions are subject to kinetic restrictions [20], as illustrated in Fig. 1(b). Note that, for a SFM, all singlet correlations are destroyed within the interface region [they decay on the short length scale $\lambda\!\!\!^{-}_J = \hbar/(p_{F2} - p_{F3}) \ll \hbar v_{F2,3}/\Delta \equiv \xi_{0\eta}$ [21]]. The boundary conditions are formulated in terms of the normal-state scattering matrix (S matrix) of the interface [19], which has the general form

$$\hat{S} = \hat{\varphi}\begin{bmatrix} \hat{R}_{11} & \vec{T}_{12} & \vec{T}_{13} \\ \vec{T}_{21}^T & r_{22} & r_{23} \\ \vec{T}_{31}^T & r_{32} & r_{33} \end{bmatrix}\hat{\varphi}^\dagger. \qquad (2)$$

Here, $\hat{\varphi}$ is a diagonal matrix with $\hat{\varphi}_{11} = e^{i(\varphi/2)\sigma_3}$, $\varphi_{22} = e^{i(\varphi/2)}$, and $\varphi_{33} = e^{-i(\varphi/2)}$.

We obtain the reflection and transmission coefficients from a microscopic calculation. We consider an interface formed by a thin ($\approx \lambda\!\!\!^{-}_F$) insulating FM layer of thickness d between the SC and bulk SFM [see Fig. 1(b)], characterized by an interface potential $V_I - \vec{J}_I \cdot \vec{\sigma}$. The orientation of the exchange field $\vec{J}_I$ in the interface layer is determined by angles α and φ, with α the angle between $\vec{J}_I$ and the exchange field $\vec{J}_{\rm FM}$ of the bulk SFM [see Fig. 2(b)]. The S matrix connecting in- and outgoing amplitudes in the bulk SC and SFM is then obtained by a wave-matching technique, where the amplitudes in the interface layer are eliminated. Doing so, we obtain in the tunneling limit an S matrix of the form $\hat{R}_{11} = e^{i(\vartheta/2)\sigma_3}$, $\vec{T}_{12} = \vec{T}_{21} = (t_2 e^{i\vartheta_2/2}, t_2' e^{-i\vartheta_2/2})^T$, and $\vec{T}_{13} = \vec{T}_{31} = (t_3' e^{i\vartheta_3/2}, t_3 e^{-i\vartheta_3/2})^T$. The spin mixing ϑ angles in these expressions [3,14,19] (also called spin-dependent interfacial phase shifts [22]) and all remaining S matrix parameters are obtained from a microscopic calculation as outlined above. As such, they depend on d, V_I, α, φ, and the Fermi momenta of the three bands (we assume $|\vec{J}_I| = |\vec{J}_{\rm FM}|$). The dependence on the angle φ is made explicit in Eq. (2), while the dependence on the angle α is implicit in the r and t parameters via $t_{2,3}' \propto \sin(\alpha/2)$, $t_{2,3} \propto \cos(\alpha/2)$, and $r_{23}, r_{32} \propto \sin\alpha$. In the following we use these tunneling-limit expressions to gain insight into the physics of the problem. The results shown in the figures, however, are obtained by a full

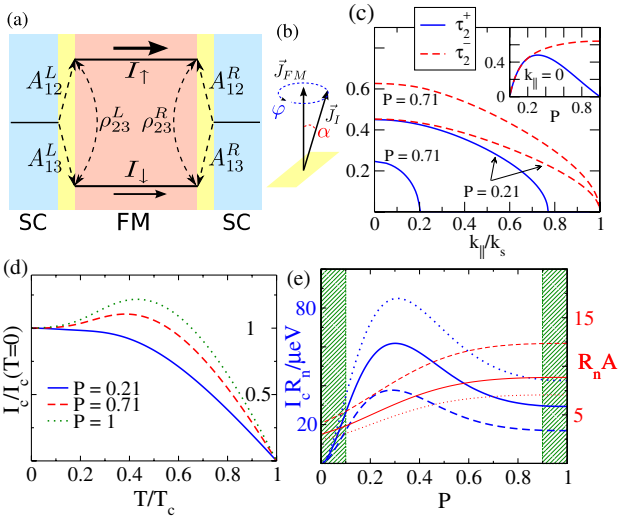

FIG. 2 (color online). (a) Josephson junction with spin-active SC/SFM interfaces formed by magnetized layers. (b) Orientation of the interface magnetization described by spherical angles α and φ. (c) The quantities $\tau_2^{\pm}$ in Eq. (7) vs $\vec{k}_\parallel$ for two polarizations P, and vs P for perpendicular impact (inset). (d) Critical current I_c vs temperature T for various polarizations P of the SFM layer. (e) I_cR_n-product and normal-state resistance R_nA as function of P for $T = 0.5T_c$, $d = \lambda\!\!\!^{-}_{F1}$, and $(V_I - J_I)/E_F = 10^{-4}$ (dotted line), 0.2 (solid line), 0.5 (dashed line). R_nA is in units of $(e^2 N_{F1} v_{F1})^{-1}$, N_{F1} being the normal-state SC density of state. $\Delta = 1.76$ meV. In all plots: $\alpha_L = \alpha_R = \pi/2$, $\varphi_L = \varphi_R$, $L = \xi_0$, $d = 5\lambda\!\!\!^{-}_{F1}$, $V_I - J_I = 0.5E_F$, $p_{F2} = 1.18p_{F1}$, unless stated otherwise. P is tuned by p_{F3}.

numerical calculation. For definiteness, we present results for parabolic electron bands with equal effective masses.

Applying these boundary conditions to a Josephson junction depicted in Fig. 2(a), and assuming bulk solutions for the QCGFs incoming from the SC electrodes, we arrive at the following system of linear equations for the f functions in the tunneling limit (labels k, $j \in \{L, R\}$ with $j \neq k$ denote the left/right interfaces):

$$\begin{bmatrix} f_2 \\ f_3 \end{bmatrix}_j^{\text{out}} = \begin{bmatrix} |r_{22}|^2 & \rho_{23} \\ \rho_{32} & |r_{33}|^2 \end{bmatrix}_j \begin{bmatrix} \beta_2 f_2 \\ \beta_3 f_3 \end{bmatrix}_k^{\text{out}} + \begin{bmatrix} A_{12} \\ A_{13} \end{bmatrix}_j. \quad (3)$$

Here, the factors $\beta_\eta = e^{-2|\varepsilon_n|L/v_{\perp\eta}}$, where $L \gg \lambda_J$ is the junction length, $\varepsilon_n = (2n+1)\pi k_B T$ the Matsubara frequency, $v_{\perp\eta}$ the Fermi velocity component along the interface normal, and $\eta \in \{2, 3\}$ the band index, arise from the decay of the f functions in the SFM layer. As depicted in Fig. 2(a), coupling between the SFM spin bands is provided by the quantity (for our model $r_{23} r_{32}^*$ is real)

$$[\rho_{23}]_j = [r_{23} r_{32}^* e^{i2\varphi}]_j = [\rho_{32}]_j^*, \quad (4)$$

while the inhomogeneity in Eq. (3), $[A_{1\eta}]_j$, can be interpreted as a pair transmission amplitude from the SC into spin band η of the SFM through the interface j. It reads

$$[A_{1\eta}]_j = -i\pi \frac{\text{sgn}(\varepsilon_n)}{1-\delta^2} [(B_\eta + C_\eta) t_\eta t'_\eta \Delta e^{i(\chi \pm \varphi)}]_j, \quad (5)$$

$$B_\eta = \tau_\eta^+ / \Omega_n, \qquad C_\eta = \tau_\eta^- |\varepsilon_n| / \Omega_n^2, \quad (6)$$

$$\tau_\eta^\pm = \sin\vartheta_\eta \pm \sin(\vartheta_\eta - \vartheta), \qquad \delta = \Delta \sin(\vartheta/2)/\Omega_n, \quad (7)$$

where $\Omega_n = \sqrt{\varepsilon_n^2 + \Delta^2}$, χ is the order parameter phase of the corresponding SC, and the $+(-)$ sign in $\chi \pm \varphi$ corresponds to $\eta = 2(3)$. Note that $t_\eta t'_\eta \propto \sin(\alpha)$, implying that the generation of triplet correlations relies on $\alpha \neq 0$.

In Fig. 2(c) we show $\tau_\eta^\pm$, Eq. (7), for the majority spin band ($\eta = 2$) as a function of $k_\parallel$. For large enough $k_\parallel$, τ_2^+ vanishes in contrast to τ_2^-. This region of $\vec{k}_\parallel$ values allows for transmission into only a single spin band of the FM [see Fig. 1(b)]. With increasing spin polarization $P = (p_{F2} - p_{F3})/(p_{F2} + p_{F3})$, it extends over a larger range of $\vec{k}_\parallel$ values, eventually spanning the entire Fermi surface for a half metal. At the same time the maximal value of τ_2^+ decreases to zero, as demonstrated in the inset in Fig. 2(c), where the parameters $\tau_2^\pm$ are shown for normal impact as function of P. The $\tau_\eta^\pm$ enter the B_η and C_η terms in Eq. (6), which exhibit different temperature (T) dependencies due to the additional $|\varepsilon_n|$ term in C_η [7]. This interplay leads to an intriguing change in the T dependence of the Josephson current, plotted in Fig. 2(d). For high P, a nonmonotonic behavior is observed similar to that for a half metal [3,11], due to the dominant C_2 term, whereas for smaller P the term arising from B_2 leads to a monotonic decay with increasing T. As a result, the bump in $I_c(T)$ disappears with decreasing polarization.

In Fig. 2(e) we plot the $I_c R_n$ product as a function of P (left scale). The variation of the normal-state resistance R_n with P (right scale) cannot account for the variation of I_c. The critical current is suppressed for small P due to small spin mixing angles [see Fig. 2(c)], and for high P due to reduction of conductivity in the minority spin band. We thus predict a maximum critical current in a SFM junction for intermediate $P \sim 0.3$. We caution that in the hatched regions in Fig. 2(e)there are additional processes, not included in our model; e.g., for small P spin coherence leads to singlet amplitudes in the FM.

We now discuss intriguing effects associated with the angles $\varphi_{L,R}$ [see Eqs. (4) and (5) and Fig. 2(b)]. In Fig. 3(a) we plot the spin-resolved current-phase relation (CPR) [23] for a high transparency junction ($d = 0.25\lambda_{F1}$) as a function of $\Delta\chi = \chi_R - \chi_L$ for two values of $\Delta\varphi = \varphi_R - \varphi_L$. Clearly, there is a nontrivial modification of the CPR in the presence of $\Delta\varphi$. We find that the CPR can be well described by the leading Fourier terms in $\Delta\varphi$,

$$I_\sigma \approx I_{\text{cp}} - I_{0\sigma} \sin(\Delta\chi_\sigma + \sigma\Delta\varphi), \quad (8)$$

where $\sigma = +(-)1$ for spin $\uparrow(\downarrow)$. Here, $I_{0\sigma}$ [shown in Fig. 3(b)] and $\Delta\chi_\sigma$ are renormalized due to multiple transmission processes. The first term in Eq. (8) describes a special type of multiple transmission process, which we call "crossed pair" (cp) transmission, shown in Fig. 1(a). It is a result of singlet-triplet mixing and triplet rotation induced by the interfaces. Here two singlet Cooper pairs are effectively recombined coherently into two triplet pairs that propagate in different spin bands. Similar processes recombining a higher (but even) number of pairs will also contribute. The phase associated with these processes comes from $[A_{12}A_{13}]_L[A_{12}A_{13}]_R^*$ factors with $A_{1\eta}$ from Eq. (5), and is given by multiples of $(\Delta\chi + \Delta\varphi) + (\Delta\chi - \Delta\varphi) = 2\Delta\chi$. Consequently, I_{cp} is independent of $\Delta\varphi$ and π periodic in $\Delta\chi$, as shown in Fig. 3(b) (solid line). It is also obvious that I_{cp} is spin symmetric; i.e., it carries a charge current, but no spin current. We find that transfer processes with an even number of pairs, but nonzero total spin, are in contrast to the cp transmission strongly suppressed. Contributions to the second term in Eq. (8) come

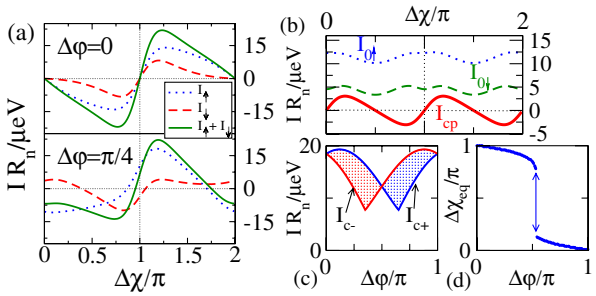

FIG. 3 (color online). (a) Spin-resolved and total CPR for $\Delta\varphi = 0$ and $\pi/4$. (b) Coefficients I_{cp} and $I_{0\sigma}$ of Eq. (8) vs $\Delta\chi$. (c) Critical current in positive (I_{c+})/negative (I_{c-}) bias direction vs $\Delta\varphi$. (d) The equilibrium phase difference $\Delta\chi_{\text{eq}}$ vs $\Delta\varphi$ varies from π to 0. In all plots $T = 0.2T_c$, $d = 0.25\lambda_{F1}$, $P = 0.21$. Other parameters as in Fig. 2.

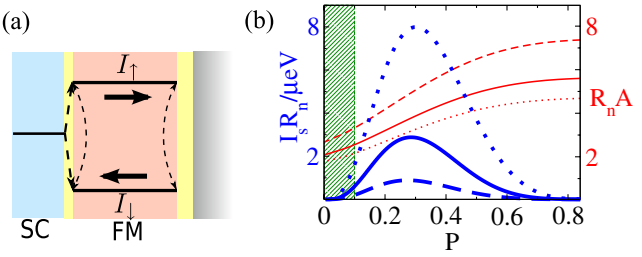

FIG. 4 (color online). (a) Setup with only one SC electrode. (b) Spin-supercurrent I_s vs P for various $(V_I - J_I)/E_F = 10^{-4}$ (dotted line), 0.2 (solid line), 0.5 (dashed line). R_nA refers to the normal-state resistance of the SC/FM interface. $d = \lambda_{F1}$; other parameters as in Fig. 2.

from processes that transmit one more Cooper pair in one of the spin bands compared to the other, including single pair transmission. It is therefore spin dependent in magnitude [see Fig. 3(b)] and shows $\Delta\varphi$ phase shifts with opposite signs for opposite spins. The relative phase between the two terms in Eq. (8) leads to surprising measurable effects for finite $\Delta\varphi$ and intermediate P. First, we find a difference in the positive (I_{c+}) and negative (I_{c-}) bias critical charge currents, as shown in Fig. 3(c). This is also directly visible in Fig. 3(a), where the maximum and minimum current have a different absolute value. Second, we find a shift of the equilibrium phase $\Delta\chi_{\rm eq}$ for the charge current, as shown in Fig. 3(d) (the jump as a function of $\Delta\varphi$ is associated with multiple local free energy minima). We note that in the tunneling limit Eq. (8) reduces to $I_\sigma \approx -I_{0\sigma} \cdot \sin(\Delta\chi + \sigma\Delta\varphi)$, and the equilibrium phase shift is present as long as $I_{0\uparrow} \neq I_{0\downarrow}$.

Another remarkable consequence of a nonzero $\Delta\varphi$ is observed for a setup shown in Fig. 4(a), when a SFM is coupled via a spin-active interlayer to a single SC on the left, and is terminated by a magnetic surface on the right. All quasiparticles are reflected at the surface, leading to a zero charge current. However, not all of them are reflected back into their original spin band since spin-flip reflections [ρ_{23} in Eq. (4)] mediate interactions between the two bands, and, remarkably, a pure spin supercurrent remains. In this case, both terms in Eq. (8) vanish as they are related to direct transmission. Instead, the leading term for the spin supercurrent is of second order in $\Delta\varphi$, $I \propto \sin(2\Delta\varphi)$, resulting from the phases picked up when a triplet Cooper pair reflects at the right interface [24]. The maximal spin current, defined as $I_s = \max_{\Delta\varphi} I(\Delta\varphi)$, is plotted in Fig. 4(b) as a function of spin polarization. Note that it vanishes both for $P \to 0$ and $P \to 1$, since it requires the presence of two bands, and is maximum for intermediate P.

This pure spin current can be tuned by an external microwave field that couples to the magnetization of the right surface in Fig. 4(a), and thus leads to a time dependent $\Delta\varphi(t)$. A high degree of control can be achieved by manufacturing a surface layer using a different magnetic material, preferably magnetized perpendicular to the bulk FM, thus optimizing external tunability. As $\Delta\varphi(t)$ acts as a time dependent superconducting phase, we predict in addition to a spin accumulation in the FM a measurable ac spin supercurrent, analogous to the ac charge Josephson current in a voltage biased junction.

In summary, we have presented a study of heterostructures between singlet superconductors and strongly spin-polarized ferromagnets. We have found that the Josephson effect markedly differs from that for a fully polarized material or for a ferromagnet with a weak spin band splitting. We discussed the importance of the phase shift between single pair and crossed two-pair transfer processes that leads to measurable anomalous junction behavior. We have also found that a pure spin supercurrent is induced in a strongly polarized ferromagnet coupled to one singlet superconducting electrode, and have proposed a way of measuring this effect.

We thank T. Löfwander for stimulating discussions.

[1] F. S. Bergeret *et al.*, Rev. Mod. Phys. **77**, 1321 (2005).
[2] A. I. Buzdin, Rev. Mod. Phys. **77**, 935 (2005).
[3] M. Eschrig *et al.*, Phys. Rev. Lett. **90**, 137003 (2003).
[4] A. F. Volkov *et al.*, Phys. Rev. Lett. **90**, 117006 (2003).
[5] J. Kopu *et al.*, Phys. Rev. B **69**, 094501 (2004).
[6] R. S. Keizer *et al.*, Nature (London) **439**, 825 (2006).
[7] M. Eschrig *et al.*, J. Low Temp. Phys. **147**, 457 (2007).
[8] M. Houzet *et al.*, Phys. Rev. B **76**, 060504(R) (2007).
[9] V. Braude and Yu. Nazarov, Phys. Rev. Lett. **98**, 077003 (2007).
[10] Y. Asano *et al.*, Phys. Rev. Lett. **98**, 107002 (2007).
[11] M. Eschrig *et al.*, Nature Phys. **4**, 138 (2008).
[12] V. Buzdin *et al.*, Pis'ma Zh. Eksp. Teor. Fiz. **35**, 147 (1982) [JETP Lett. **35**, 178 (1982)]; Z. Radović *et al.*, Phys. Rev. B **68**, 014501 (2003).
[13] V. V. Ryazanov *et al.*, Phys. Rev. Lett. **86**, 2427 (2001); T. Kontos *et al.*, *ibid.* **89**, 137007 (2002).
[14] T. Tokuyasu *et al.*, Phys. Rev. B **38**, 8823 (1988).
[15] A. Schmid and G. Schön, J. Low Temp. Phys. **20**, 207 (1975); J. W. Serene *et al.*, Phys. Rep. **101**, 221 (1983).
[16] G. Eilenberger, Z. Phys. **214**, 195 (1968); A. I. Larkin and Y. N. Ovchinnikov, Zh. Eksp. Teor. Fiz. **55**, 2262 (1968) [Sov. Phys. JETP **28**, 1200 (1969)].
[17] A. Shelankov, J. Low Temp. Phys. **60**, 29 (1985); A. Shelankov and M. Ozana, Phys. Rev. B **61**, 7077 (2000).
[18] M. Eschrig, Phys. Rev. B **61**, 9061 (2000).
[19] A. Millis, D. Rainer, and J. A. Sauls, Phys. Rev. B **38**, 4504 (1988); M. Fogelström, *ibid.* **62**, 11 812 (2000); E. Zhao *et al.*, *ibid.* **70**, 134510 (2004).
[20] I. Žutić and O. T. Valls, Phys. Rev. B **61**, 1555 (2000); K. Halterman and O. T. Valls, *ibid.* **66**, 224516 (2002); J. Linder and A. Sudbø, *ibid.* **75**, 134509 (2007).
[21] The condition for treating the singlet components within QC theory is $\lambda_J^2 \gg \xi_{0\eta}\lambda_{F\eta} \gg \lambda_{F\eta}^2$.
[22] A. Brataas *et al.*, Phys. Rev. Lett. **84**, 2481 (2000); D. Huertas-Hernando *et al.*, *ibid.* **88**, 047003 (2002); A. Cottet and W. Belzig, Phys. Rev. B **72**, 180503 (2005).
[23] A. A. Golubov *et al.*, Rev. Mod. Phys. **76**, 411 (2004).
[24] For a similar effect in a triplet-SC/*I*/triplet-SC junction see P. M. R. Brydon and D. Manske, arXiv:0901.4096.